Supporting Information: Voltage-Switchable Phosphate Recovery Using Magnetite-Coated Electrodes in Hybrid Capacitive Deionization

Kelly E. Matuszewski,[†] Elias M. Kallon,[†] Lauren Valentino,[*,‡] and Vinayak P. Dravid[*,†,¶]

[†]*Department of Materials Science and Engineering, Northwestern University, Evanston, Illinois 60208, United States*

[‡]*Applied Materials Division, Argonne National Laboratory, Lemont, Illinois 60439, United States*

[¶]*The NUANCE Center, Northwestern University, Evanston, Illinois 60208, United States*

E-mail: lvalentino@anl.gov; v-dravid@northwestern.edu

Downloaded from pubs.acs.org/aeecco/article-supplement/5472178/pdf/ee6c00609_si_001/ by guest on 23 November 2026

Contents

1 Material Analysis **S3**

2 H-CDI Results **S4**

3 Cyclic Voltammetry **S11**

4 Mechanism Analysis **S12**

Downloaded from pubs.acs.org/aeecco/article-supplement/5472178/pdf/ee6c00609_si_001/ by guest on 23 November 2026

Sections 1 contains additional results from the Materials Analysis subsection, with scanning electron microscopy of the bare carbon cloth (CC) and powder X-ray diffraction (pXRD) spectra for the Fe_3O_4 as synthesized. Section 2 contains additional results from the H-CDI Results subsection, and contains the conditions used for all of the H-CDI experiments, along with in-line pH results, cycle 25 ICP-OES results, bare CC H-CDI results, current profile data, cumulative P capture and recovery, P selectivity versus N, and integrated charge and charge efficiency. Section 3 contains additional results from the Cyclic Voltammetry subsection, and contains the CV results for each pH condition, along with analysis of the redox peak position as a function of pH. Section 4 contains additional results from the Mechanism Analysis subsection, and contains the unfitted XPS spectra for each region of interest, the fitted XPS spectra and the proposed relative compositions of binding states, and XRD results evaluating stability of the magnetite phase.

1 Material Analysis

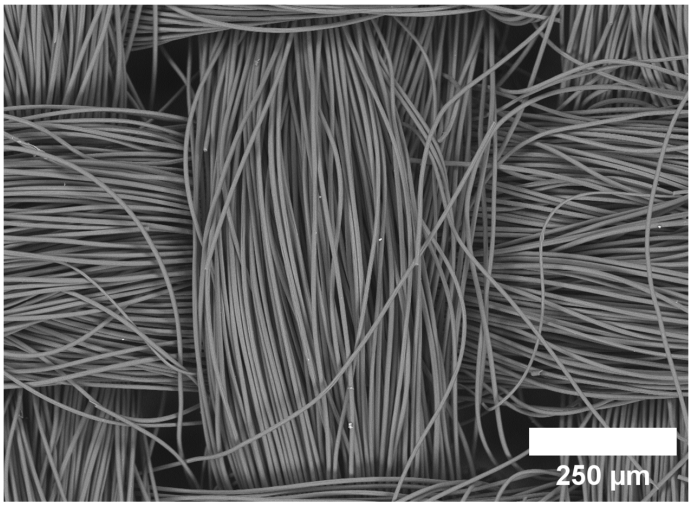


Figure S1: SEM micrograph of bare carbon cloth electrode using the backscattered electron detector for elemental contrast, showing a uniform carbon substrate.

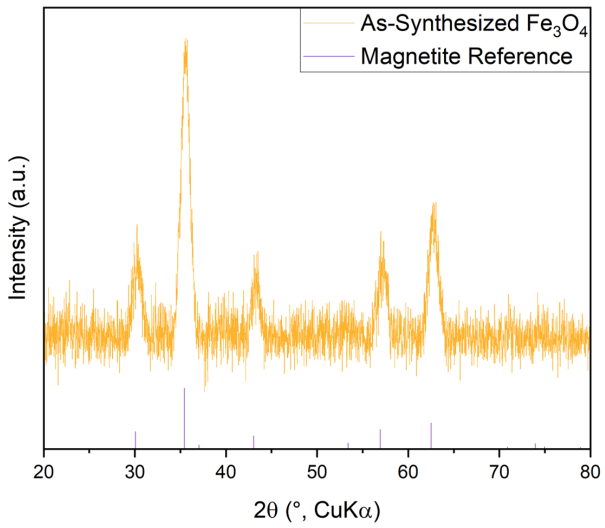


Figure S2: pXRD pattern of the as synthesized Fe_3O_4@CC electrode, showing the presence of magnetite. Magnetite reference acquired in MDI JADE (CSD#294, entry 98-000-0294)

Downloaded from pubs.acs.org/aeecco/article-supplement/5472178/pdf/ee6c00609_si_001/ by guest on 23 November 2026

2 H-CDI Results

Table S1: Experimental conditions used during H-CDI experiments to evaluate the effects of initial pH, P concentration, and flow rate (residence time).

pH Effects			**Concentration Effects**			**Residence Time Effects**		
pH	**P Conc. (mg L^{-1})**	**Flow (mL/min)**	**pH**	**P Conc. (mg L^{-1})**	**Flow (mL/min)**	**pH**	**P Conc. (mg L^{-1})**	**Flow (mL/min)**
5.5	5.0	1.0	6.5	1.0	1.0	6.5	5.0	1.0
6.0	5.0	1.0	6.5	5.0	1.0	6.5	5.0	4.0
6.5	5.0	1.0	6.5	10.0	1.0	6.5	5.0	7.0
7.5	5.0	1.0						

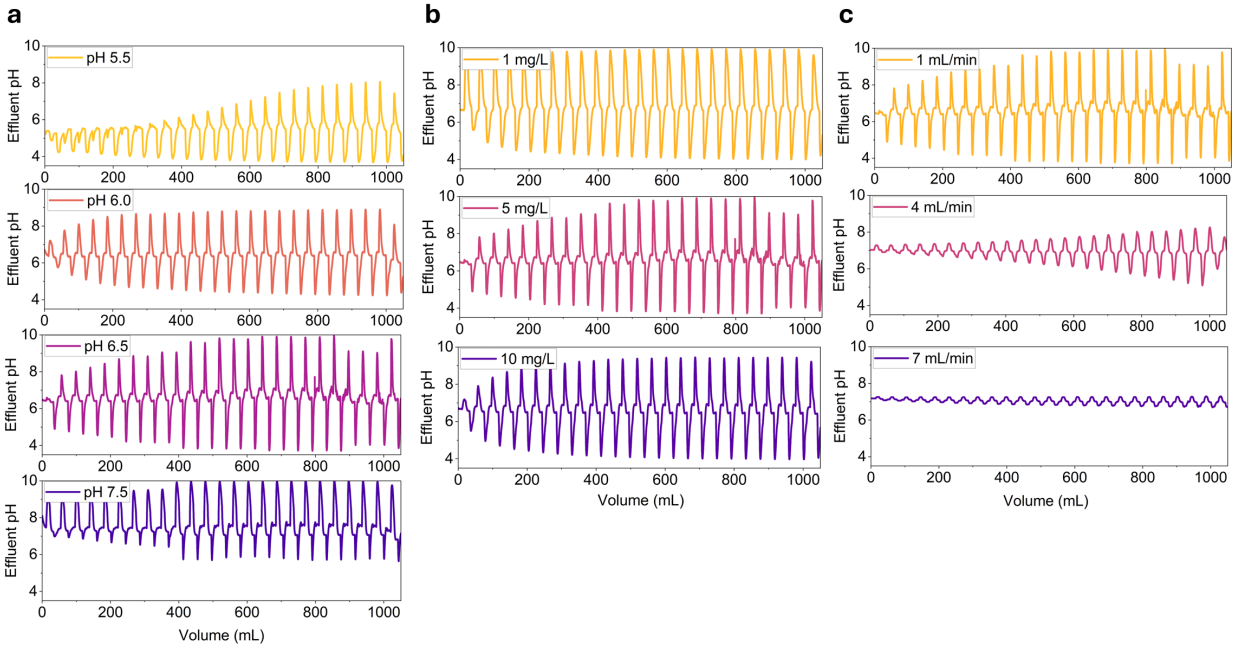


Figure S3: Results for the effluent in-line pH meter for all 25 H-CDI cycles (0 V, 1.2 V, 0 V, -1.2 V) with varying (a) initial pH, (b) initial P concentration, and (c) flow rate.

Downloaded from pubs.acs.org/aeecco/article-supplement/5472178/pdf/ee6c00609_si_001/ by guest on 23 November 2026

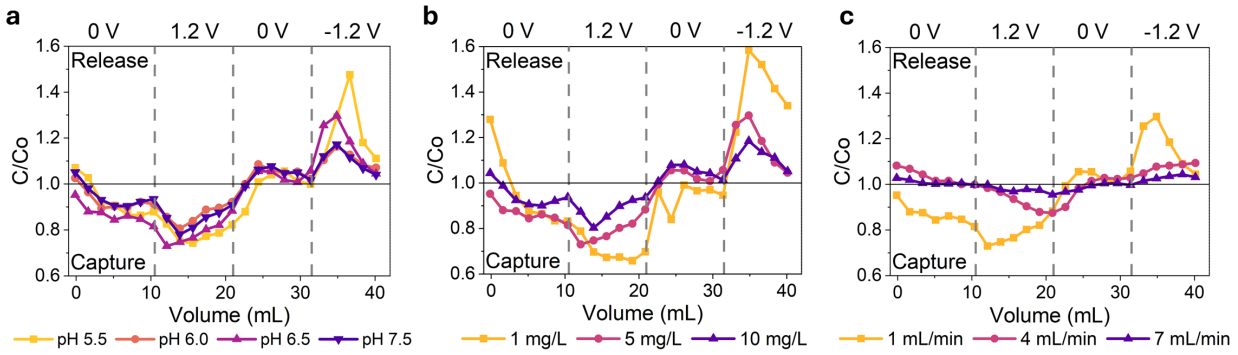


Figure S4: ICP-OES results, in terms of effluent concentration (C) divided by the initial concentration (C_0) for the 25th cycle of H-CDI P capture and release for varying (a) initial pH, (b) initial P concentration, and (c) flow rate.

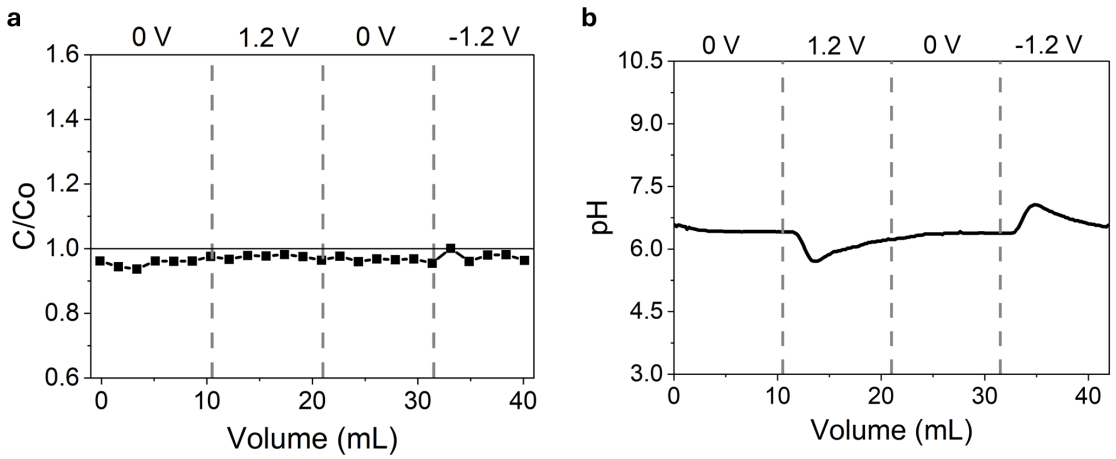


Figure S5: ICP-OES and in-line pH results for the 25th cycle of H-CDI P capture and release for a control bare CC working electrode, demonstrating the need for Fe_3O_4 for the P capture/release process.

Downloaded from pubs.acs.org/aeecco/article-supplement/5472178/pdf/ee6c00609_si_001/ by guest on 23 November 2026

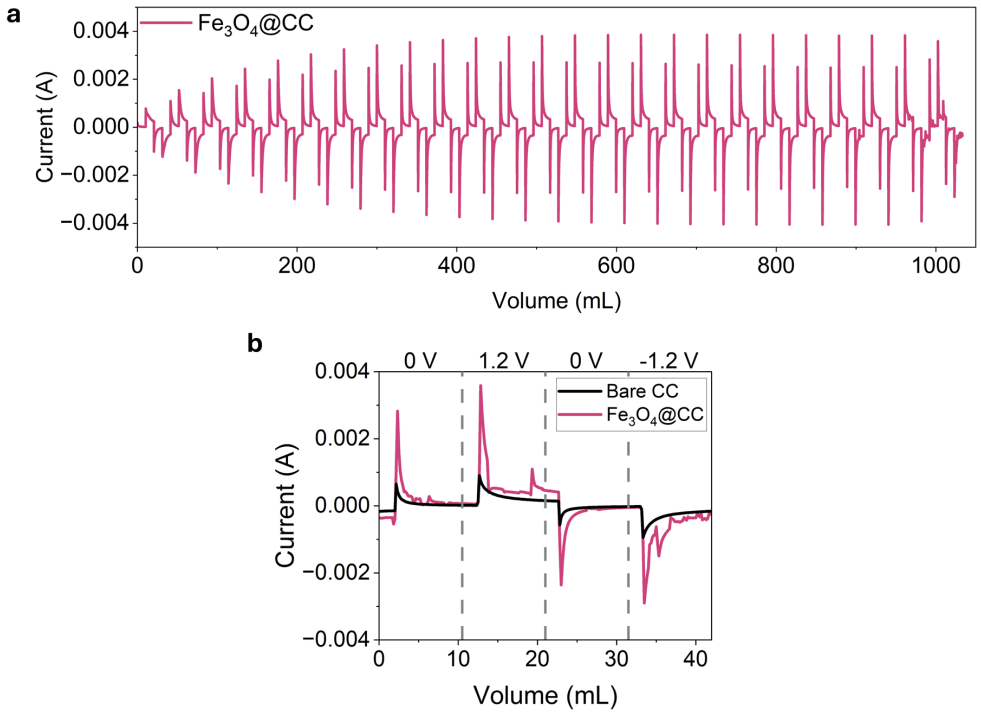


Figure S6: (a) Current profile data across all cycles for the baseline conditions (pH 6.5, 5 mg/L, 1 mL/min) for the Fe_3O_4@CC electrode. (b) Current profiles for the bare CC electrode sample and the Fe_3O_4@CC electrode sample at baseline conditions for the 25th cycle.

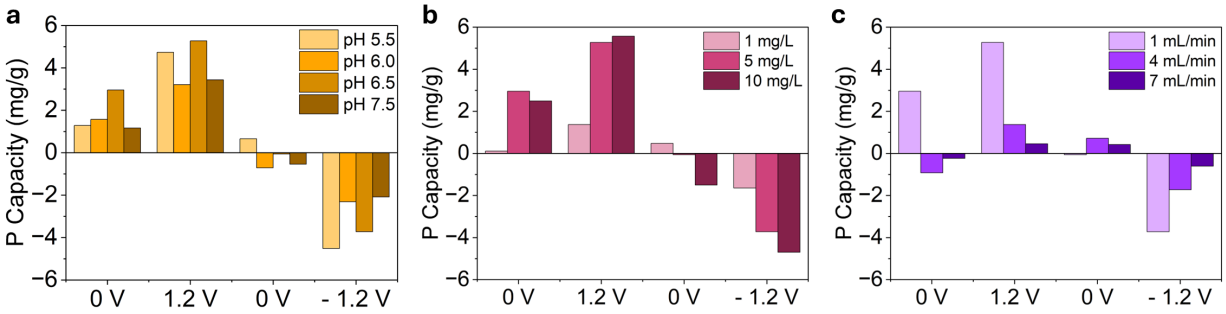


Figure S7: Capacity of P on the Fe_3O_4@CC electrode surface per g of active material for each voltage step during cycle 25 for a variety of (a) initial pH values, (b) initial P concentrations, and (c) flow rates.

Downloaded from pubs.acs.org/aeecco/article-supplement/5472178/pdf/ee6c00609_si_001/ by guest on 23 November 2026

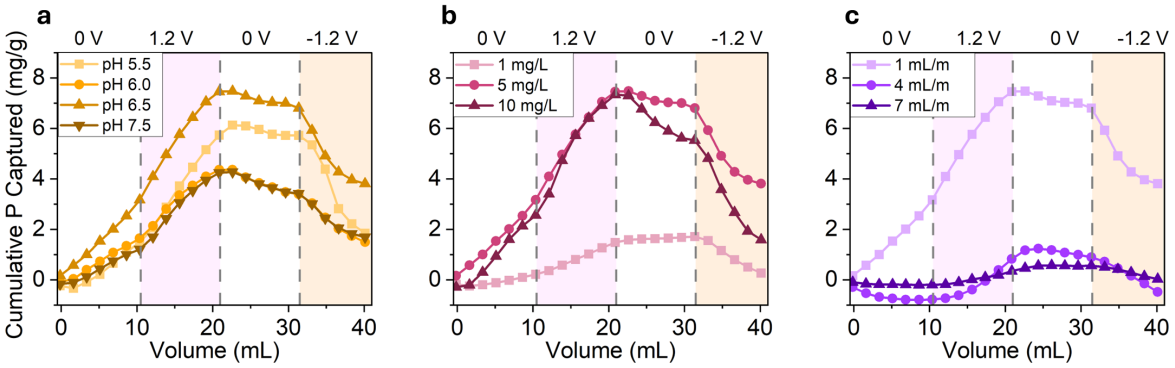


Figure S8: Cumulative P captured onto the Fe_3O_4@CC surface across one H-CDI cycle, in units of mg P per g of Fe_3O_4, for varying (a) initial pH, (b) initial P concentration, and (c) flow rate. This demonstrates the rapid rise in capture/release when the voltage steps are initiated, and the incomplete recovery of P based on the amount left on the electrode surface at the end of the cycle.

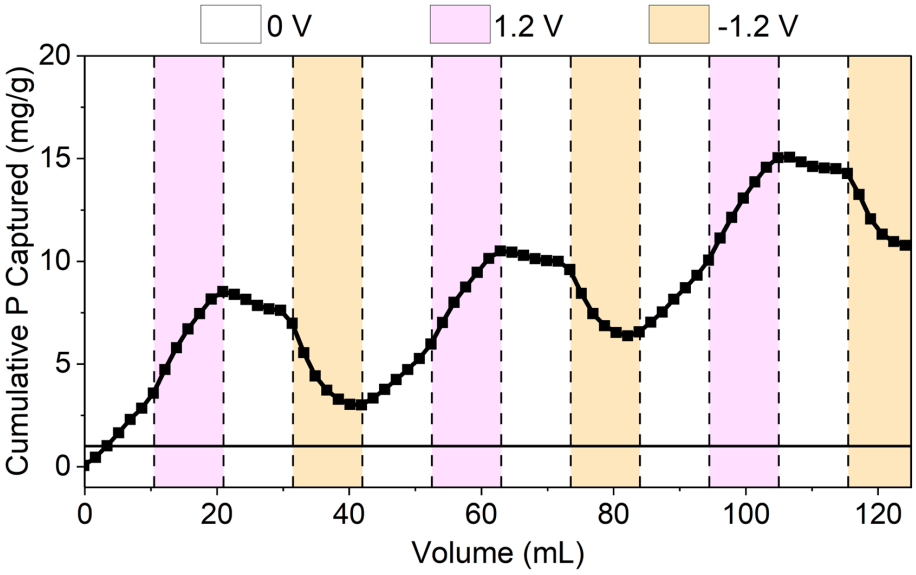


Figure S9: Cumulative P captured on the Fe_3O_4@CC electrode across H-CDI cycles 23-25, with baseline operating conditions of 5 mg P / L, pH 6.5, at 1 mL/min.

Downloaded from pubs.acs.org/aeecco/article-supplement/5472178/pdf/ee6c00609_si_001/ by guest on 23 November 2026

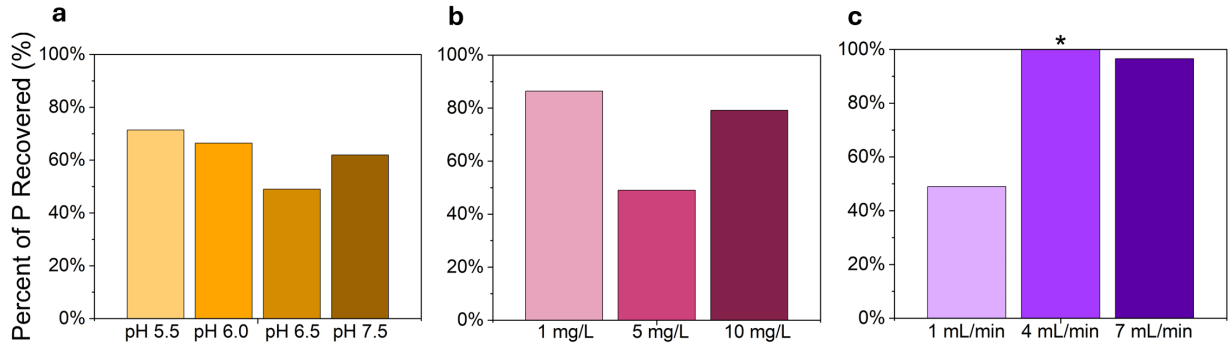


Figure S10: Percent of P recovered at the end of the 25th H-CDI cycle from Figure S8 as a function of (a) initial pH, (b) initial P concentration, and (c) flow rate. An asterisk denotes the 4 mL/min dataset, which reaches 124% apparent recovery; this value above 100% likely reflects measurement uncertainty from integrating small concentration differences via ICP-OES or minor carryover of P release from the preceding adsorption step rather than true net desorption exceeding capture.

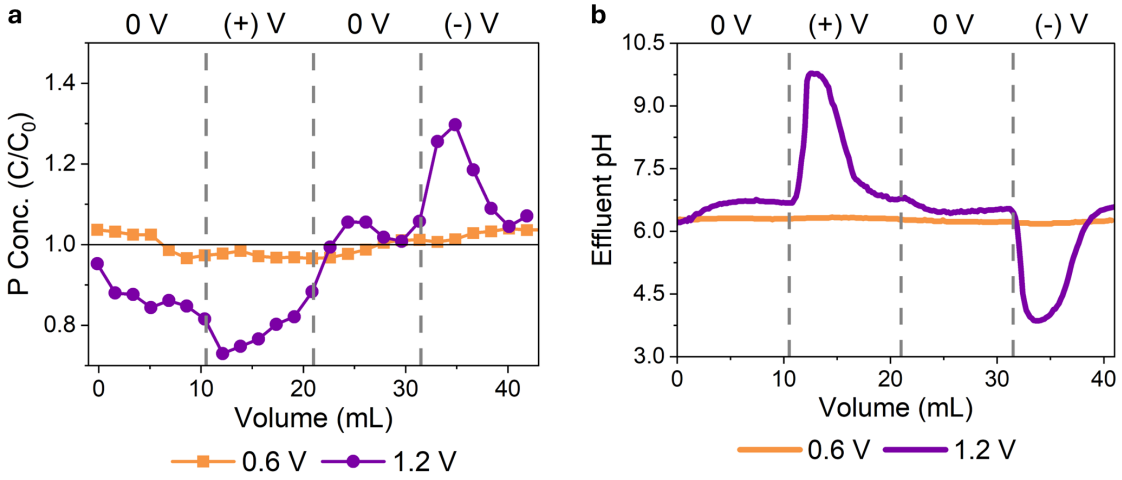


Figure S11: (a) ICP-OES and (b) in-line pH results for the 25th H-CDI cycle for the dataset from Figure S4 and Figure 3a,d (1.2 V, pH 6.5, 5 mg L^{-1}, 1 mL/min), compared to new data which lowered the applied voltage to 0.6 V (pH 6.5, 5 mg L^{-1}, 1 mL/min) showing that the voltage applied largely affects P capture and pH response.

For the Ion Chromatography data presented in Figure S12, potassium hydroxide (KOH) was used as the eluent, with a concentration of 15 mM from 0 to 9 min, followed by 35 mM

Downloaded from pubs.acs.org/aeecco/article-supplement/5472178/pdf/ee6c00609_si_001/ by guest on 23 November 2026

KOH from 9 to 20 min. The flow rate was maintained at 0.25 mL min^{-1}, with an injection volume of 10 µL and a column temperature of 35 °C. The suppressor current was set to 25 mA. All anionic species were eluted within 15 min under these chromatographic conditions. Note: Chloride data were excluded due to background leaching from $FeCl_3 \cdot 6\,H_2O$ precursor during Fe_3O_4 synthesis. P and N data are unaffected by this artifact.

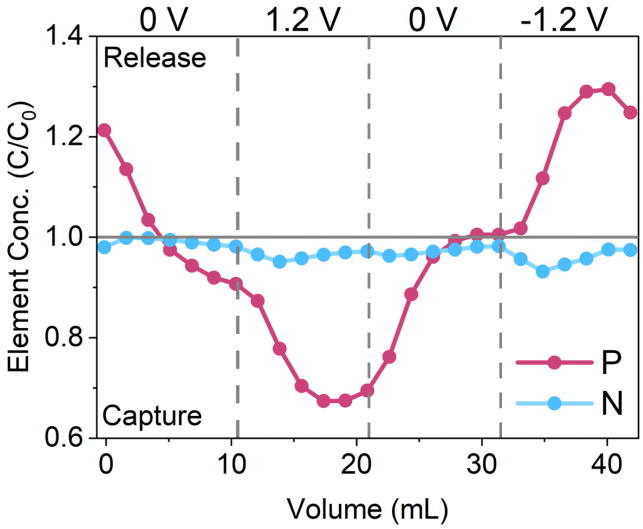


Figure S12: IC results, in terms of effluent concentration (C) divided by the initial concentration (C0) for the 25th cycle of H-CDI P and N capture and release for the P selectivity study.

For the calculation of integrated charge and charge efficiency as presented in Figure S13, the equations below are used. Here, Q is the integrated charge, I is the current, t is time, Λ is charge efficiency, z is the charge of the ion, F is Faradays constant, and $n_{P,ads/rem}$ is the number of phosphate ions captured or released during the voltage step.

$$Q = \int I dt \tag{S1}$$

$$\Lambda = \frac{zFn_{p,ads/rel}}{Q} \tag{S2}$$

Downloaded from pubs.acs.org/aeecco/article-supplement/5472178/pdf/ee6c00609_si_001/ by guest on 23 November 2026

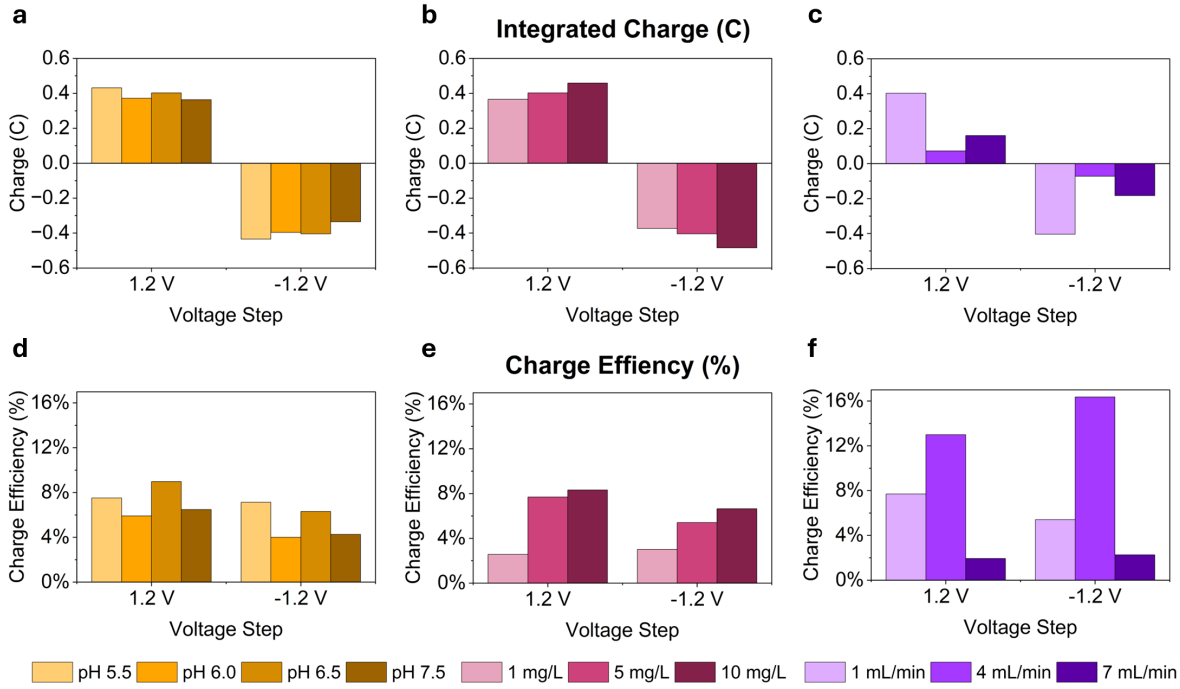


Figure S13: Integrated charge (C) data for cycle 25 for each H-CDI experiment for varying (a) initial pH, (b) initial P concentration, and (c) flow rate. Charge efficiency calculations for cycle 25 for each H-CDI experiment for varying (d) initial pH, (e) initial P concentration, and (f) flow rate.

Downloaded from pubs.acs.org/aeecco/article-supplement/5472178/pdf/ee6c00609_si_001/ by guest on 23 November 2026

3 Cyclic Voltammetry

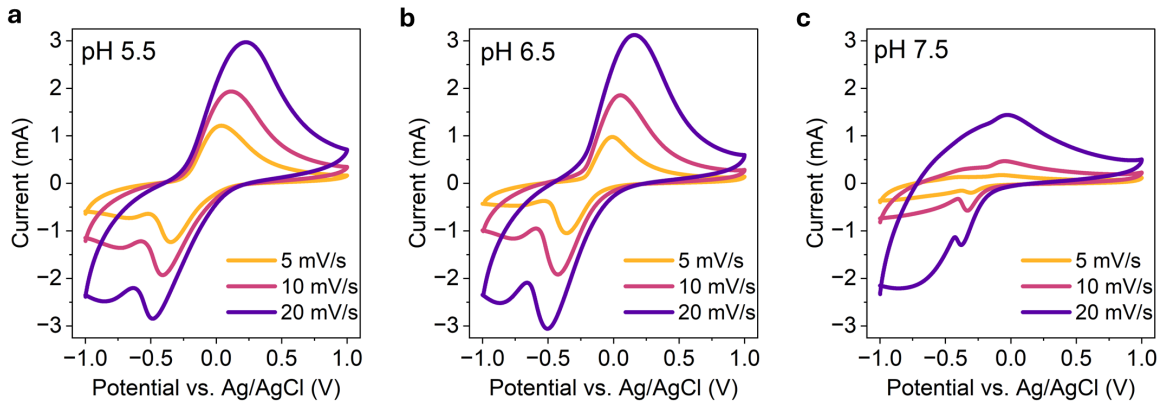


Figure S14: CV results for Fe_3O_4@CC electrodes in 50 mM H_2PO_4 at varying scan rates to evaluate the corresponding redox response in a solution with an initial (a) pH 5.5, (b) pH 6.5, and (c) pH 7.5.

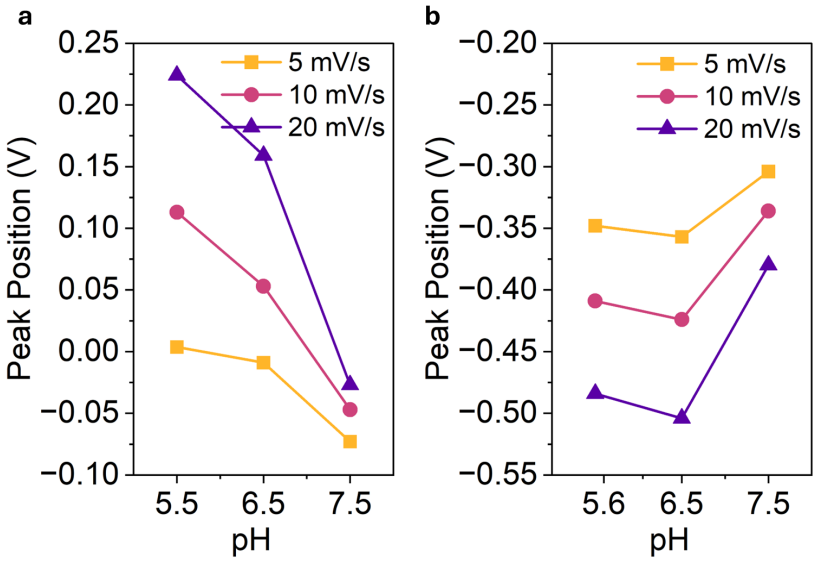


Figure S15: Redox peak position versus initial pH at varying scan rates derived from CV results (Figure S14) for Fe_3O_4@CC electrodes in 50 mM H_2PO_4 for the (a) anodic and (b) cathodic peaks. This data was used to derive $E_{1/2}$ seen in Figure 4d.

Downloaded from pubs.acs.org/aeecco/article-supplement/5472178/pdf/ee6c00609_si_001/ by guest on 23 November 2026

4 Mechanism Analysis

For XPS analysis, peak fitting was carried out using the Smart background option in Avantage. The Fe 2p1/2 doublet (725 eV) was excluded from quantitative fitting, and therefore the oxidation-state assignments were based on the 2p3/2 region alone to prevent obscuring the Fe^{2+}/Fe^{3+} distinction. The normalized component fraction in Equation S1 represents the area of a fitted Fe 2p component relative to the summed fitted area used for the comparison. Fractions obtained for the components near 710 and 712 eV were used to track relative changes in Fe 2p line shape between samples.

$$f_i = \frac{A_i}{\sum_{j=1}^{n} A_j} \tag{S3}$$

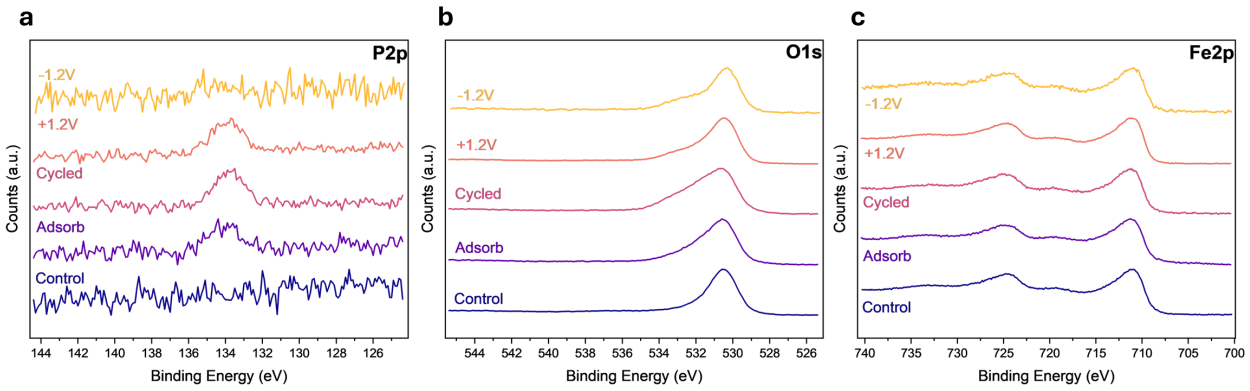


Figure S16: XPS spectra for Fe_3O_4@CC electrodes with the following initial conditions: (1) pristine control with no voltage P exposure, (2) exposure to 5 mg L^{-1} of P at pH 6.5 with no applied voltage or flow, (3) exposure to only 1.2 V for one H-CDI cycle, (4) exposure to only -1.2 V for one H-CDI cycle, and (5) exposure to 25 full H-CDI cycles. Shown for the (a) P 2p, (b) O 1s, and (c) Fe 2p regions.

Downloaded from pubs.acs.org/aeecco/article-supplement/5472178/pdf/ee6c00609_si_001/ by guest on 23 November 2026

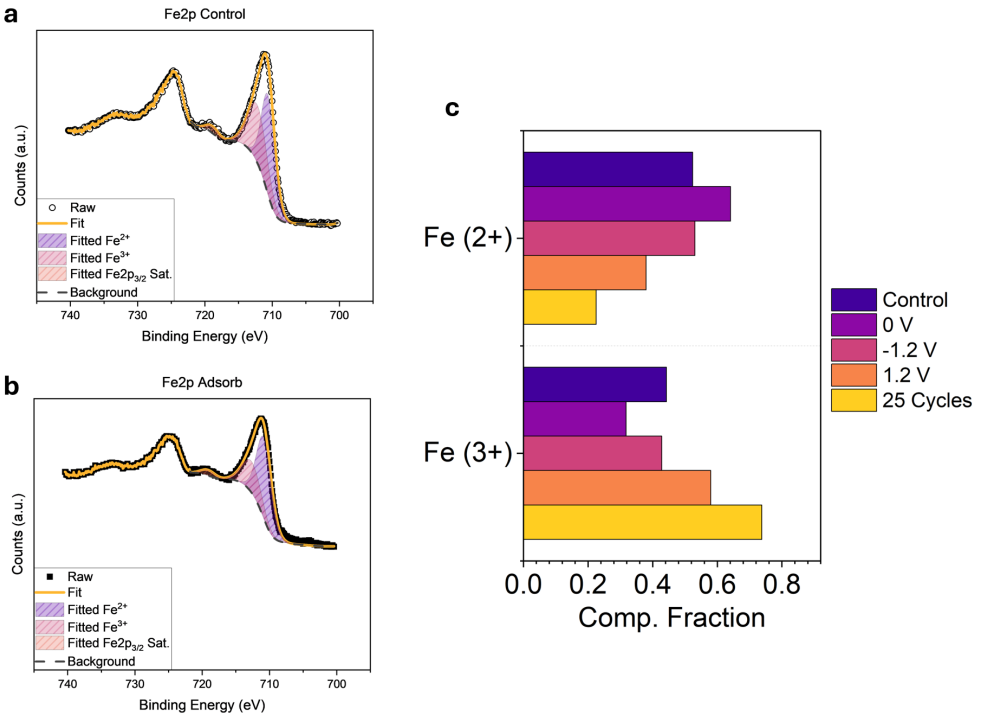


Figure S17: Fitted XPS spectra, for the (a) pristine control with no voltage P exposure, (b) exposure to 5 mg L^{-1} of P at pH 6.5 with no applied voltage or flow, focused on the Fe 2p regime. (c) Compositional fractions, based on fitted spectra, for the two oxidation states of Fe, with a notable increase in Fe^{3+} for the Fe_3O_4@CC sample exposed to 25 H-CDI cycles.

Downloaded from pubs.acs.org/aeecco/article-supplement/5472178/pdf/ee6c00609_si_001/ by guest on 23 November 2026

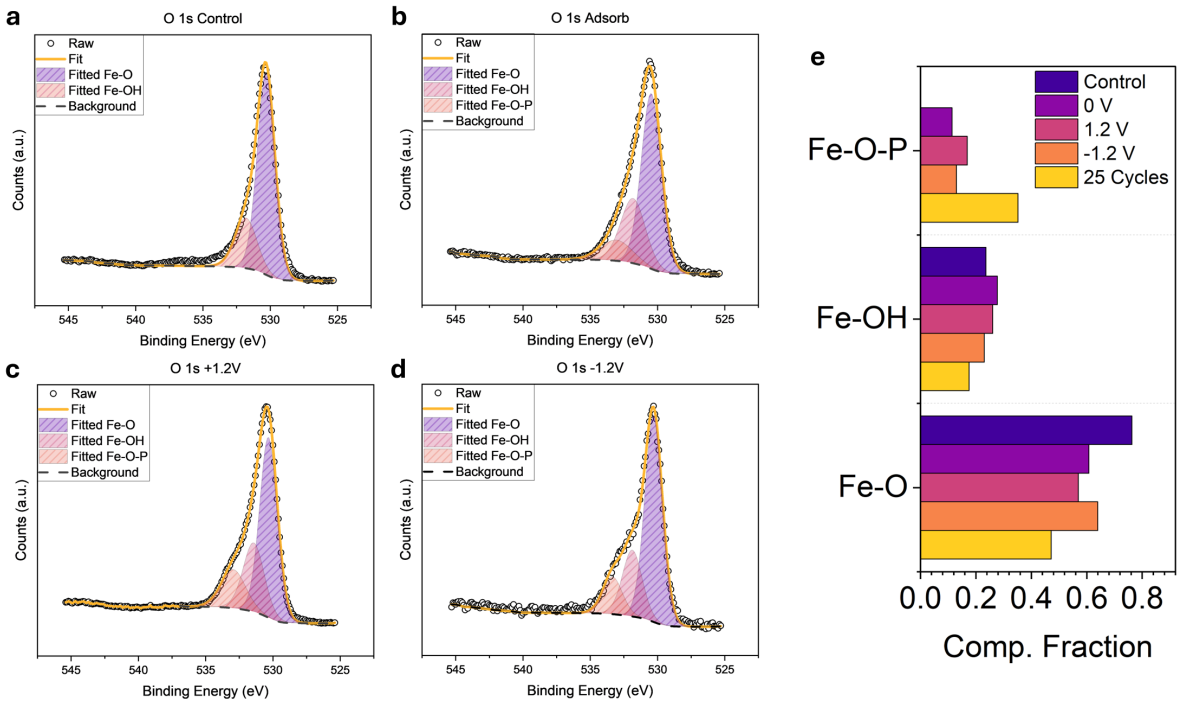


Figure S18: Fitted XPS spectra in the O 1s regime for the (a) pristine control with no voltage P exposure, (b) exposure to 5 mg L^{-1} of P at pH 6.5 with no applied voltage or flow, focused on the O 1s regime, (c) exposure to only 1.2 V for one H-CDI cycle, and (d) exposure to only -1.2 V for one H-CDI cycle. (e) Compositional fractions for selected oxygen bonding states for each pre-treatment, with a notable increase in Fe−O−P composition for the Fe_3O_4@CC sample exposed to 25 H-CDI cycles.

For XRD measurements in Figure S19, the diffraction patterns were collected using a step size of 0.06° and a scan rate of 5°/min. Carbon cloth samples were mounted on a low-background Si wafer to minimize background contributions from the substrate. The magnetite reference was acquired in MDI JADE, CSD 294, entry 98-000-0294.

Downloaded from pubs.acs.org/aeecco/article-supplement/5472178/pdf/ee6c00609_si_001/ by guest on 23 November 2026

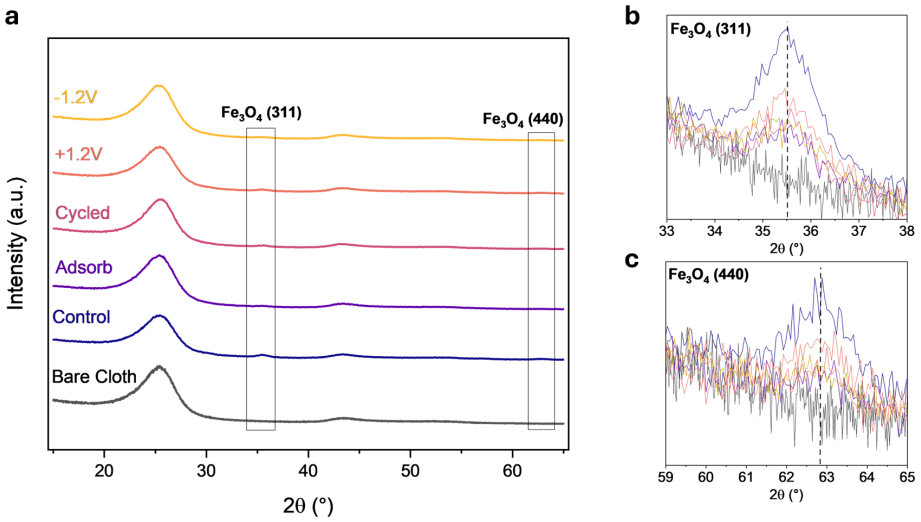


Figure S19: (a) XRD measurements for Fe_3O_4@CC samples including an as-synthesized control with no voltage P exposure, electrode exposed to 5 mg/L of P at pH 6.5 with no applied voltage or flow, electrode exposed to only 1.2 V for one H-CDI cycle, electrode exposed to only -1.2 V for one H-CDI cycle, and an electrode exposed to 25 cycles of baseline conditions. Additionally, a bare CC was evaluated to confirm the large amorphous carbon peak. An inset of the XRD data near the (b) (311) and (c) (440) magnetite peaks.

The written out equations proposed to be occurring at the Fe_3O_4@CC electrode during voltage application in the H-CDI cell can be found below. These include the iron reduction (Equation S4), iron oxidation (Equation S5), surface site protonation (Equation S6), and surface site deprotonation (Equation S7).

$$\equiv \mathrm{Fe(III)}{-}\mathrm{OH} + \mathrm{e}^- \longrightarrow \equiv \mathrm{Fe(II)}{-}\mathrm{OH} \tag{S4}$$

$$\equiv \mathrm{Fe(II)}{-}\mathrm{OH} \longrightarrow \equiv \mathrm{Fe(III)}{-}\mathrm{OH} + \mathrm{e}^- \tag{S5}$$

$$\equiv \mathrm{Fe(III)}{-}\mathrm{OH} + \mathrm{H}^+ \longrightarrow \equiv \mathrm{Fe(III)}{-}\mathrm{OH}_2^+ \tag{S6}$$

$$\equiv \mathrm{Fe(II)}{-}\mathrm{OH} \longrightarrow \equiv \mathrm{Fe(II)}{-}\mathrm{O}^- + \mathrm{H}^+ \tag{S7}$$

Downloaded from pubs.acs.org/aeecco/article-supplement/5472178/pdf/ee6c00609_si_001/ by guest on 23 November 2026